CROSSTALK REDUCTION IN SPHERICAL LOUDSPEAKER ARRAYS VIA DECOUPLED ENCLOSURES

Pierre Lecomte[1]

[1] *Ecole Centrale de Lyon, CNRS, Universite Claude Bernard Lyon 1, INSA Lyon, LMFA, UMR5509, 69130,Ecully, France*

This paper is a revised version of the authors' submitted manuscript that was peer-reviewed by at least two anonymous reviewers.

Abstract

Compact spherical loudspeaker arrays enable the synthesis of controllable directivities using loudspeakers distributed over a rigid spherical surface. However, most existing designs rely on a shared rear enclosure, leading to acoustic coupling between loudspeakers. This coupling requires the use of multiple-input multiple-output crosstalk cancellation systems. In this paper, we propose an alternative approach based on the physical decoupling of loudspeakers through a parametric enclosure design using spherical fraction geometries. This design significantly reduces acoustic coupling, allowing the control problem to be simplified to a set of independent single-input single-output equalization filters. A prototype consisting of 18 loudspeakers arranged according to a Popov cubature rule is designed and manufactured. Acoustic crosstalk is experimentally characterized using laser Doppler vibrometry. Results show an average crosstalk reduction of approximately 20 dB compared to a reference spherical array with shared enclosure. Simulated directivity patterns, based on a spherical cap model combined with the measured acoustic coupling, demonstrate that this per-driver equalization is sufficient to synthesize directive beams.

Keywords: *spherical loudspeaker array, directivity control, acoustic crosstalk, loudspeaker design, spherical harmonics*

1. Introduction

Sound sources with controllable directivity based on compact Spherical Loudspeaker Arrays (SLA)s have been extensively studied in recent years. Different approaches have been proposed, either relying on the description of sound fields using Spherical Harmonics (SHs) [1], [2], or on radiation mode control [3]. In most prototypes, the loudspeakers are mounted on a rigid spherical structure and share a common rear enclosure. While this design facilitates construction and improves low-frequency efficiency, it also introduces acoustic coupling between transducers. As a result, independent control of the loudspeaker velocities requires the use of a crosstalk cancellation system, typically implemented as a Multiple-Input Multiple-Output (MIMO) filter matrix with a computational complexity of $\mathcal{O}(N^2)$, where N is the number of loudspeakers. For regular polyhedron geometries, this crosstalk matrix can be expressed in the spherical harmonics domain, where it exhibits a sparse or approximately diagonal structure [4], thereby reducing the computational burden. In this paper, we propose an alternative approach in which each loudspeaker is acoustically decoupled from its neighbors through a spherical fraction enclosure design. This strongly reduces acoustic crosstalk so that only per-driver equalization is required, reducing the control complexity to $\mathcal{O}(N)$. This decoupling comes at the expense of low-frequency efficiency, since each driver is now loaded by a small individual enclosure rather than a large shared volume. This trade-off is deliberately accepted here in the context of a do-it-yourself design targeting consumer-grade 3D printers, whose limited build volume precludes large spherical shells. Each enclosure is instead fixed to the closed-box volume recommended by the driver datasheet, and the array is assembled by gluing individual closed-box enclosures into a spherical geometry, much like closed-box cabinets are combined to form line arrays. A parametric CAD framework is proposed for arbitrary spherical layouts. It is implemented as part of the library SMALL^{+} [1], which extends the SMALL framework [5] to compact SLAs. The paper is organized as follows: Section 2 presents the parametric CAD approach; Section 3 the 18-loudspeaker Popov prototype [6]; Section 4 the crosstalk characterization; Section 5 the beam synthesis and equalization; and

Corresponding author: *pierre.lecomte@ec-lyon.fr.*

[1] `https://gitlab.pmcs2i.ec-lyon.fr/plecomte/small`

Section 6 the results, before conclusions in Section 7.

2. Parametric CAD using python and openSCAD

The library SMALL+[1] provides open-hardware solutions for building compact spherical microphone arrays (SMA) [5] and compact SLAs with a 3D printer and some soldering and assembling. This section details the parametric CAD approach to design the compact SLA.

2.1. Partitioning of the sphere into zones using a spherical Voronoi diagram

We start with a spherical mesh using N nodes. To create the adjacent spherical sector geometries, the sphere is divided into cells centered on the nodes. This is achieved using a Voronoi diagram algorithm applied to the surface of a sphere [7]. The algorithm determines the vertices of the cells on the spherical surface, with each node located at their centers. An example of the result is shown in fig. 1. Note that an extra point is added to the mesh to produce an additional cell for cable management and a threaded nut mount (in green in fig. 1). For this cell, the vertices can be moved toward its center to adjust its size. This

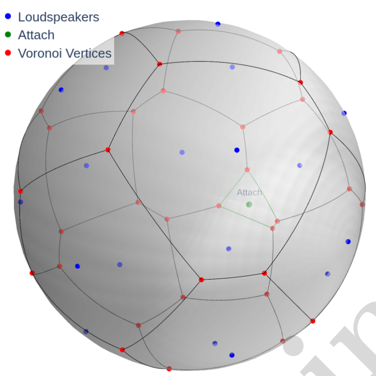

Figure 1: The Voronoi cells are generated from a spherical mesh (in blue), and the Voronoi vertices are shown in red. An additional point (in green) is included to serve as the attachment for the compact SLA stand.

algorithm is implemented in Python on a unit radius sphere using the SphericalVoronoi function from the scipy.spatial package.

2.2. Creation of closed-box loudspeakers using OpenSCAD

Based on the coordinates of each node of a cell, a parametric OpenSCAD[2] model constructs the loudspeaker enclosure with a succession of Boolean operations on solids as shown in fig. 2. The successive operations are detailed hereafter: One denotes the radius of the compact SLA as r_0. For the i-th enclosure:

1. A polyhedron in the form of a pyramid with a polygonal base is generated. The apex of the pyramid is placed at the origin of the coordinate system (the center of the compact SLA), while the vertices of the polygonal base correspond to the vertices of the cell extrapolated on a sphere of radius $1.5 \times r_0$ (fig. 2(a)).

2. The solid resulting from the Boolean intersection with a sphere of radius r_0 is then created. Then, a sphere of internal radius r_i is subtracted from it using a Boolean difference operation (fig. 2(b)).

3. The resulting solid is then hollowed out to form the enclosure, leaving walls of constant thickness and the opening used to mount the loudspeaker driver. This is achieved by subtracting a tool solid that fills the target inner volume of the enclosure, shown in purple in fig. 2(c).

4. The final enclosure is obtained (fig. 2(d)).

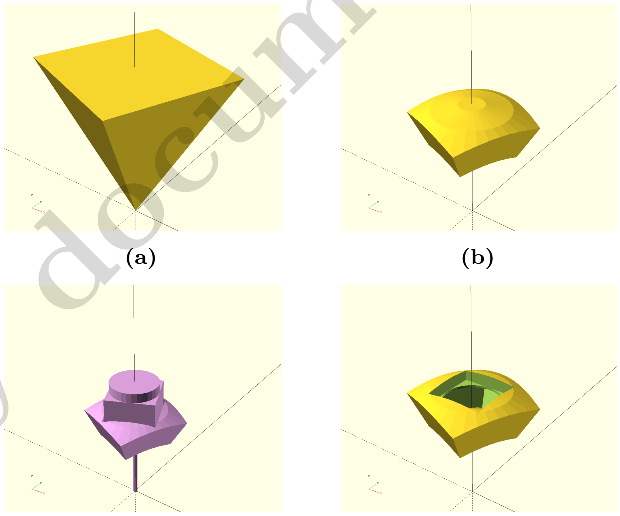

(a) (b) (c) (d)

Figure 2: The different steps in the construction of a loudspeaker enclosure from the coordinates of the vertices of a cell.

2.3. Adjustments of enclosure volume

Except for Platonic configurations, spherical partitions into identical geodesic regions are not possible, making identical enclosure geometries difficult to achieve. Furthermore, the additional cell used for the speaker stand attachment and cable management also disrupts the uniformity of the geometries. As a result, the enclosure volumes vary, which can affect their acoustic response. However, the procedure described in Section 2.2 allows for the adjustment of the internal radius r_i for each enclosure, thereby controlling the enclosure volume to match a desired value V_b, relative to the speaker's equivalent compliance volume V_{as} [8].

3. Prototype fabrication

Each enclosure is 3D-printed by fused deposition modeling (FDM) or stereolithography. Figure 3 shows a

[2] `https://openscad.org/`

(a)

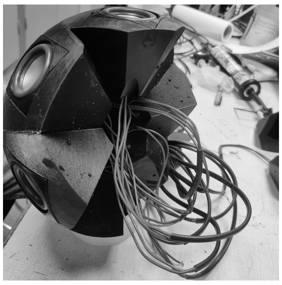

(b)

(c)

Figure 3: (a) The spherical fraction shape loudspeakers are printed using an FDM 3D printer. (b) The SLA is assembled by gluing. (c) Final result

compact SLA of radius $r_0 = 0.1$ m using $N = 18$ 2" Aura Sound NSW2-326-8A drivers on a Popov cubature exact up to degree $L = 3$ [6]. The aperture angle of each driver is $\alpha = 28°$. Each driver is mounted from outside and held by a spacer. The enclosures ($V_b \approx 0.1$ L) are filled with foam and bonded with a polyurethane adhesive ensuring airtightness. The inner cavity gathers the cables, routed through the additional housing labeled "Attach" in fig. 1, which also holds a threaded insert for the stand.

4. Acoustic crosstalk measurement

The acoustic coupling is characterized by membrane vibration measurements using a laser Doppler vibrometer (LDV). The LDV is focused on the n-th membrane while each of the N loudspeakers is successively driven by a sine sweep, yielding the voltage-to-velocity transfer functions to that membrane. The procedure is repeated for all loudspeakers. For each frequency, one then constructs an acoustic crosstalk matrix, denoted $\mathbf{M} \in \mathbb{C}^{N \times N}$, which relates the commanded loudspeaker velocities $\mathbf{v}$ to the resulting membrane velocities $\mathbf{u}$ as

$$\mathbf{u} = \mathbf{M}\mathbf{v}. \tag{1}$$

Here, the driving signal of each loudspeaker is set proportional to its commanded velocity v_n, and $\mathbf{M}$, estimated from the measured voltage-to-velocity transfer functions, maps this command to the actual membrane velocity. The diagonal entries of $\mathbf{M}$ thus correspond to the direct electro-mechanical response of each loudspeaker, while the off-diagonal terms quantify the acoustic coupling between neighboring transducers. The results of the crosstalk measurements are

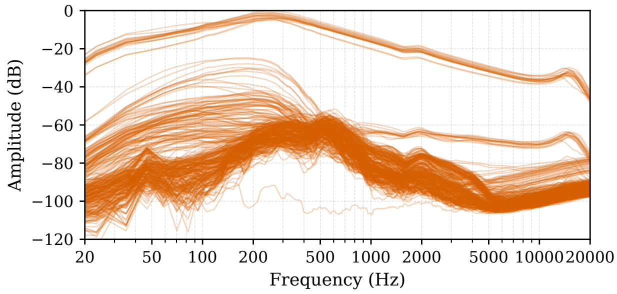

(a)

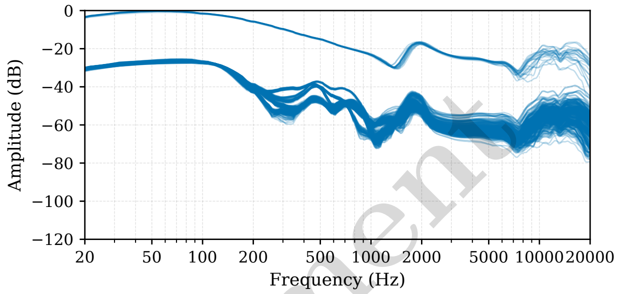

(b)

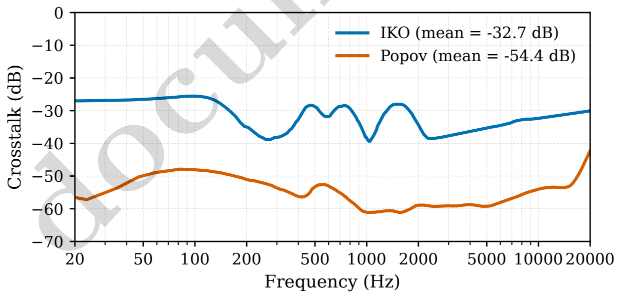

(c)

Figure 4: The measured acoustic crosstalk is maximum-normalized. (a) The frequency responses of all entries of the crosstalk matrix $\mathbf{M}$ are shown for the proposed prototype. (b) The corresponding measurements are shown for the IKO array. (c) The average crosstalk is defined as the ratio between the mean off-diagonal and diagonal terms of $\mathbf{M}$. All curves are displayed with 1/3-octave smoothing.

presented in fig. 4. Fig. 4(a) shows the frequency responses of the entries of the matrix $\mathbf{M}$ for the proposed prototype. The bundle of curves with higher amplitudes corresponds to the diagonal terms of $\mathbf{M}$, while the remaining curves correspond to the off-diagonal terms, i.e., the acoustic coupling between loudspeakers. Among the latter, a few outliers exhibit a noticeably higher coupling. These are assumed to originate from enclosures that are not perfectly airtight, in particular at the cable pass-through hole, resulting in a residual acoustic coupling through the remaining inner volume of the array. For comparison, the same measurement performed on the IKO [2] is shown in fig. 4(b). A comparison of the direct (diagonal) responses in fig. 4(a) and fig. 4(b) also illustrates the low-frequency tradeoff discussed in Section 1: the direct response of the proposed decoupled design extends less toward low frequencies than that of the shared-enclosure IKO. This difference is not solely due to the enclosure strategy, as the IKO uses larger 6.3-inch drivers, against 2-inch drivers for the present prototype, which further favors its low-frequency radiation. To quantify the crosstalk, the ratio between the average off-diagonal and diagonal terms is computed versus frequency in fig. 4(c). The proposed prototype reaches an average of -54 dB, about 20 dB below the IKO array. This is considered low enough to neglect the crosstalk, which, as discussed in Section 5.3, reduces the equalization complexity from $\mathcal{O}(N^2)$ to $\mathcal{O}(N)$.

5. Directivities simulation

5.1. Spherical cap modeling

One uses a spherical cap model for directivity synthesis [1], [2]. Let us consider the n-th spherical cap at location (θ_n, ϕ_n) on a rigid unit sphere, where $\theta \in [0, \pi]$ is the colatitude and $\phi \in [0, 2\pi)$ the azimuth. The velocity is constant and equals to unity on the cap whereas it is null everywhere else. The SH expansion of such velocity pattern is given by [1]:

$$v_{lm}(\theta_n, \phi_n) = \hat{A}_l Y_{lm}(\theta_n, \phi_n), \tag{2}$$

where Y_{lm} are the 4-pi normalized real SH of degree l and order m and

$$\hat{A}_l = \begin{cases} \cos(\frac{\alpha}{2}) P_l(\cos(\frac{\alpha}{2})) - P_{l-1}(\cos(\frac{\alpha}{2})) & l > 0 \\ 1 - \cos(\frac{\alpha}{2}) & l = 0 \end{cases}. \tag{3}$$

In Eq. 3, P_l are the Legendre Polynomials of degree l, and α is the aperture angle of the cap. By using N spherical caps at the surface of a rigid sphere of radius r_0, with v_n the velocity of the n-th cap, one obtains the acoustic pressure SH expansion coefficients at radius r, denoted p_{lm} as:

$$p_{lm}(kr, kr_0) = i\rho_0 c \frac{h_l(kr)}{h'_l(kr_0)} \sum_{n=1}^{N} v_n \hat{A}_l Y_{lm}(\theta_n, \phi_n). \tag{4}$$

In Eq. (4), $i = \sqrt{-1}$, $k = \omega/c$ is the wavenumber with ω the angular frequency, $\rho_0 = 1.2$ kg/m^3 is the air density, $c = 345.4$ m/s is the speed of sound in air corresponding to the ambient temperature during the measurements, h_l are the spherical Hankel functions of the second kind, and h'_l their derivative with respect to the argument. By expressing all the coefficients up to maximal degree L, one can use a matrix formulation:

$$\tilde{\mathbf{p}} = i\rho_0 c \mathbf{H}\mathbf{A}\mathbf{Y}^T \mathbf{v}, \tag{5}$$

where $\tilde{\mathbf{p}} = [p_{00}, \cdots, p_{lm}, \cdots, p_{LL}]^T \in \mathbb{C}^{(L+1)^2}$ are the reconstructed pressure SH coefficients. The matrix $\mathbf{H} \in \mathbb{C}^{(L+1)^2 \times (L+1)^2}$ is diagonal,

$$\mathbf{H} = \operatorname{diag}\Big[\eta_0, \cdots, \underbrace{\eta_l, \cdots, \eta_l}_{2l+1 \text{ times}}, \cdots, \eta_L\Big], \tag{6}$$

with

$$\eta_l = \frac{h_l(kr)}{h'_l(kr_0)}. \tag{7}$$

Similarly, $\mathbf{A} \in \mathbb{R}^{(L+1)^2 \times (L+1)^2}$ is diagonal,

$$\mathbf{A} = \operatorname{diag}[\hat{A}_0, \cdots, \underbrace{\hat{A}_l, \cdots, \hat{A}_l}_{2l+1 \text{times}}, \cdots, \hat{A}_L]. \tag{8}$$

Finally, $\mathbf{Y} \in \mathbb{R}^{N \times (L+1)^2}$ is the matrix of SHs at the loudspeaker directions and $\mathbf{v} = [v_1, \cdots v_N]^T \in \mathbb{C}^N$ are the cap velocities.

5.2. Inverse problem resolution

From the target pressure SH coefficients at radius r, denoted $\mathbf{p}$, we seek the source velocities $\mathbf{v}$ that reproduce them through the forward model of Eq. (5). Since the array uses N loudspeakers to control only $(L+1)^2 < N$ pressure coefficients, the forward problem is underdetermined: infinitely many velocity vectors $\mathbf{v}$ satisfy $\tilde{\mathbf{p}} = \mathbf{p}$. Among them, we seek the one of minimum energy, which leads to the constrained minimization problem

$$\min_{\mathbf{v}} \ \|\mathbf{v}\|_2^2 \quad \text{subject to} \quad i\rho_0 c \mathbf{H}\mathbf{A}\mathbf{Y}^T \mathbf{v} = \mathbf{p}. \tag{9}$$

Solving Eq. (9) with the method of Lagrange multipliers yields the minimum-norm solution $\mathbf{v} = \mathbf{G}^\dagger \mathbf{p}$, where $\mathbf{G} = i\rho_0 c \mathbf{H}\mathbf{A}\mathbf{Y}^T$ is the forward operator and $(\cdot)^\dagger$ denotes the Moore–Penrose pseudo-inverse.

Since $\mathbf{H}$ and $\mathbf{A}$ are square, diagonal and invertible, $\mathbf{G}^\dagger$ simplifies to

$$\mathbf{G}^\dagger = \frac{1}{i\rho_0 c} (\mathbf{Y}^T)^\dagger \mathbf{A}^{-1} \mathbf{H}^{-1}, \tag{10}$$

so that only the pseudo-inverse of the rectangular matrix $\mathbf{Y}^T$ remains to be computed. When the loudspeakers follow a cubature rule on the sphere [6], the SH matrix satisfies the discrete orthogonality relation

$$\mathbf{Y}^T \mathbf{W} \mathbf{Y} = \mathbf{I}, \tag{11}$$

where $\mathbf{W}$ is the diagonal matrix of cubature weights. It follows that $\mathbf{Y}^T(\mathbf{W}\mathbf{Y}) = \mathbf{I}$, so the pseudo-inverse further simplifies to

$$(\mathbf{Y}^T)^\dagger = \mathbf{W}\mathbf{Y}. \tag{12}$$

The minimum-norm solution finally reads

$$\mathbf{v} = \frac{1}{i\rho_0 c} \mathbf{W}\mathbf{Y}\mathbf{A}^{-1}\mathbf{H}^{-1}\mathbf{p}. \tag{13}$$

In Eq. (13), the entries of the matrix $\mathbf{H}^{-1}$ involve

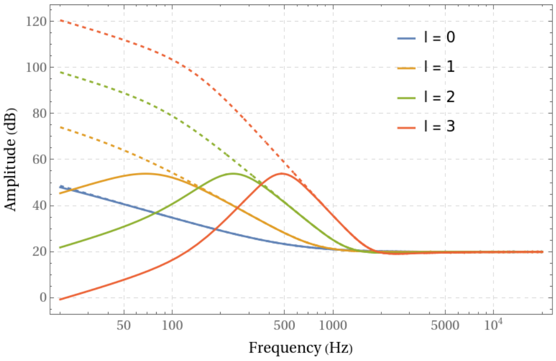

Figure 5: The inverse radial terms $\eta_{l,\lambda}^{-1}$ are shown for $\lambda = 0$ (dashed curves) and $\lambda = 10^{-3}$ (solid curves), with $r_0 = 0.1$ m and $r = 1$ m.

ratios of spherical Hankel functions and their derivatives, see Eq. (7), whose magnitude increases as the ratio r/r_0 grows, in the low-frequency regime ($k \to 0$), and with increasing harmonic degree l. This leads to unreasonably large amplification gains at low frequencies, which not only require excessive driving levels but also amplify the measurement and modeling errors of the inversion. To mitigate this issue, we introduce a regularized inverse $\mathbf{H}_\lambda^{-1} \in \mathbb{C}^{(L+1)^2 \times (L+1)^2}$ defined as

$$\mathbf{H}_\lambda^{-1} = \mathrm{diag}\Big[\eta_{0,\lambda}^{-1}, \cdots, \underbrace{\eta_{l,\lambda}^{-1}, \cdots, \eta_{l,\lambda}^{-1}}_{2l+1 \text{ times}}, \cdots, \eta_{L,\lambda}^{-1}\Big], \quad (14)$$

with

$$\eta_{l,\lambda}^{-1} = \frac{\overline{\eta_l}}{|\eta_l|^2 + \lambda^2}, \quad (15)$$

where $\overline{\eta_l}$ is the complex conjugate of η_l and λ a regularization parameter. For instance, the values of $\eta_{l,\lambda}^{-1}$ are displayed for $\lambda = 0$ and $\lambda = 10^{-3}$ in fig. 5 for $r_0 = 0.1$ m and r=1 m. This regularization parameter gives a dynamic range around ~ 35 dB.

Finally, the regularized solution then reads:

$$\mathbf{v} = \frac{1}{i\rho_0 c}\mathbf{W}\mathbf{Y}\mathbf{A}^{-1}\mathbf{H}_\lambda^{-1}\mathbf{p}. \quad (16)$$

5.3. Velocity equalization

The vector $\mathbf{v}$ from Eq. (16) gives the target velocities, related to the actual velocities $\mathbf{u}$ through Eq. 1. To obtain $\mathbf{u} = \mathbf{v}$, the driving vector is pre-equalized as

$$\tilde{\mathbf{v}} = \mathbf{M}_\lambda^{-1}\mathbf{v}, \quad (17)$$

where $\mathbf{M}_\lambda^{-1} \in \mathbb{C}^{N\times N}$ is a regularized inverse of $\mathbf{M}$. In IKO [2], this is a full $N \times N$ MIMO system of finite impulse response (FIR) filters. Here, however, the sources are assumed sufficiently decoupled so that only the individual velocities need equalizing. The matrix $\mathbf{M}$ is therefore approximated as diagonal,

$$\tilde{\mathbf{M}} = \mathrm{diag}(m_1, \ldots, m_N), \quad (18)$$

and the equalization reduces to independent scalar filters. Following the same regularization principle as for $\mathbf{H}_\lambda^{-1}$ in Eq. (14), the inverse filter matrix $\mathbf{M}_\lambda^{-1} \in \mathbb{C}^{N\times N}$ is defined as

$$\mathbf{M}_\lambda^{-1} = \mathrm{diag}\left[m_{1,\lambda}^{-1}, \cdots, m_{n,\lambda}^{-1}, \cdots, m_{N,\lambda}^{-1}\right], \quad (19)$$

with

$$m_{n,\lambda}^{-1} = \frac{\overline{m_n}}{|m_n|^2 + \lambda^2}. \quad (20)$$

It can thus be implemented only as N single-input single-output (SISO) systems with a vector of FIR filters. Finally, the equalized velocity vector $\tilde{\mathbf{v}}$ reads

$$\tilde{\mathbf{v}} = \mathbf{M}_\lambda^{-1}\mathbf{v}. \quad (21)$$

6. Results

In this section, we evaluate the prototype performance using only N equalization filters, for beam radiation synthesis using SHs up to degree $L = 3$. One chooses a target beam at $r = 1$ m as a truncated directional Dirac steered toward the direction $(\theta_s, \phi_s) = (90°, 0°)$, i.e. the horizontal plane facing forward. One then has

$$\mathbf{p} = \frac{1}{(L+1)^2} \times \left[Y_{00}(\theta_s,\phi_s),\ \cdots,\ Y_{lm}(\theta_s,\phi_s),\ \cdots,\ Y_{33}(\theta_s,\phi_s)\right]^T. \quad (22)$$

The SHs expansion of this beam over angle and frequency is visible on fig. 6(a). Next, the reproduced beam from Eq. (16) is shown in fig. 6(b) for $\lambda = 10^{-3}$. Two degradations appear with respect to the target. Below 500 Hz, the beam widens as frequency decreases, due to the regularized radial filters of Eq. (14) attenuating the higher orders; this becomes negligible beyond 500 Hz, see fig. 5. Beyond 2500 Hz, secondary lobes arise from spatial aliasing, caused by the finite number of caps and the array radius. The velocity $\mathbf{u}$ realized on the prototype is then obtained from the measured matrix $\mathbf{M}$ through Eq. (1), yielding the beam in fig. 6(c). It remains close to fig. 6(b), confirming effective decoupling, with an amplitude shaped by the loudspeaker response, see fig. 4(a). Finally, fig. 6(d) shows the beam obtained with the equalized velocities of Eq. (21): it is nearly identical to fig. 6(b), confirming that the crosstalk is negligible and that only SISO velocity equalization is needed.

7. Conclusions

We introduced a compact spherical loudspeaker array based on physically decoupled spherical fraction enclosures. In contrast to conventional SLAs relying on a shared rear cavity, the prototype strongly reduces acoustic coupling between adjacent drivers, with LDV measurements showing an average crosstalk reduction of about 20 dB compared to the IKO reference. This decoupling simplifies the control from a $\mathcal{O}(N^2)$ MIMO equalization to $\mathcal{O}(N)$ SISO equalizations, while still enabling accurate beam synthesis. The parametric CAD workflow is implemented in the SMALL^{+1} library, providing a reusable framework for compact SLAs. Future work will characterize the radiated directivities using a surrounding spherical microphone array [9].

8. Acknowledgments

The author would like to thank the PSIVA platform of the Laboratoire de Mécanique et d'Acoustique in Marseille for the LDV measurements.

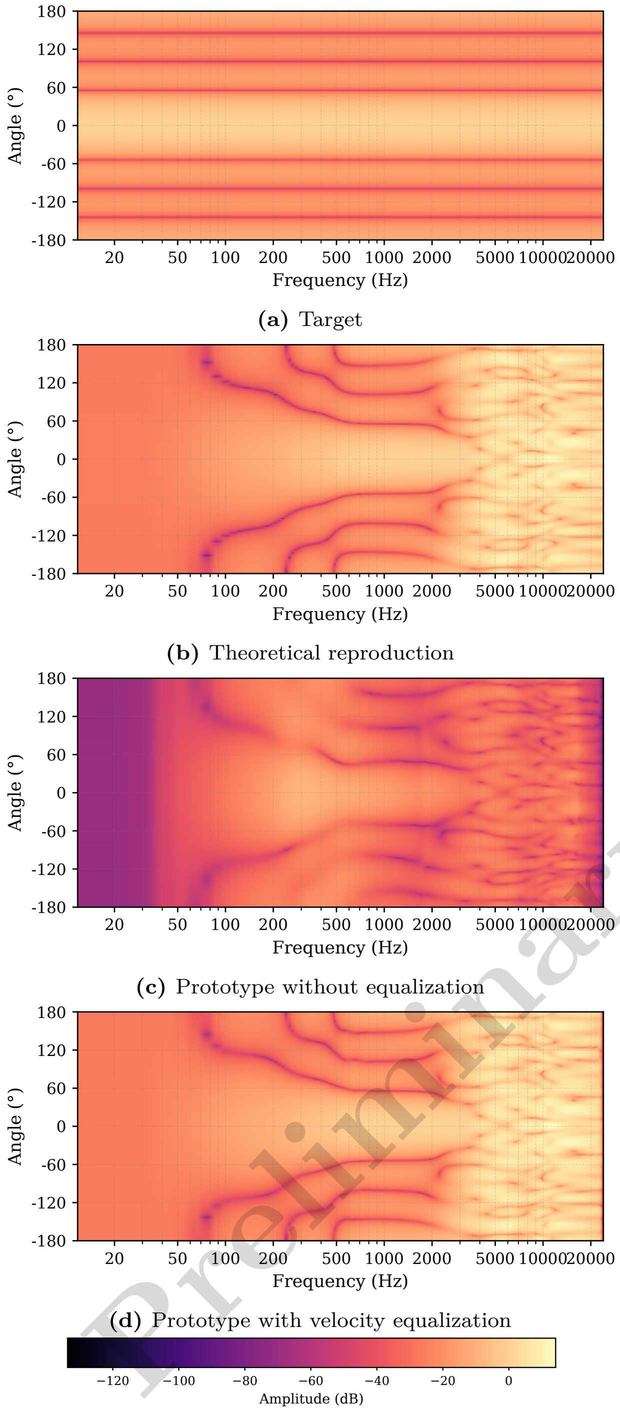

(a) Target

(b) Theoretical reproduction

(c) Prototype without equalization

(d) Prototype with velocity equalization

Figure 6: The angular-frequency maps of the synthesized beam are shown. (a) Target. (b) Theoretical reproduction. (c) Prototype without equalization. (d) Prototype with velocity equalization. For (b), (c), and (d), SH pressure coefficients are computed with Eq. (5) using $L = 20$.

References

[1] F. Zotter, A. Sontacchi, and R. Holdrich, "Modeling a spherical loudspeaker system as multipole source," *Fortschritte der Akustik*, vol. 33, no. 1, p. 221, 2007.

[2] F. Zotter, M. Zaunschirm, M. Frank, and M. Kronlachner, "A beamformer to play with wall reflections: The icosahedral loudspeaker," *Computer Music Journal*, vol. 41, no. 3, pp. 50–68, 2017.

[3] A. M. Pasqual, A. de França, J. Roberto, and P. Herzog, "Application of acoustic radiation modes in the directivity control by a spherical loudspeaker array," *Acta acustica united with Acustica*, vol. 96, no. 1, pp. 32–42, 2010.

[4] F. Zotter, H. Pomberger, and A. Schmeder, "Efficient directivity pattern control for spherical loudspeaker arrays," *Journal of the Acoustical Society of America*, vol. 123, no. 5, p. 3643, 2008. Accessed: Jun. 10, 2024.

[5] P. Lecomte, "SMALL: Spherical Microphone Arrays Little Library," in *Forum Acusticum 2023*, Turin, 2023.

[6] A. S. Popov, "Cubature Formulas on the Sphere That are Invariant Under the Transformations of the Dihedral Group of Rotations D 4," *Siberian Electronic Mathematical Reports*, vol. 17, pp. 964–970, 2020.

[7] M. Caroli, P. M. M. de Castro, S. Loriot, O. Rouiller, M. Teillaud, and C. Wormser, "Robust and Efficient Delaunay triangulations of points on or close to a sphere," INRIA, Rapport, 2009. Accessed: Sep. 1, 2025.

[8] R. H. Small, "Closed-box loudspeaker systems part I: Analysis," *Journal of the Audio Engineering Society*, vol. 20, no. 10, pp. 978–808, 1972.

[9] M. Hartenstein et al., "Sound source directivity estimation via a spherical wave decomposition of the radiated field: Application to human voice directivity measurements," in *Forum Acusticum Euronoise 2025*, 2025.